LASER INTERFEROMETER GRAVITATIONAL WAVE OBSERVATORY
- LIGO -
CALIFORNIA INSTITUTE OF TECHNOLOGY
MASSACHUSETTS INSTITUTE OF TECHNOLOGY

Technical Note	**LIGO-T2200206–v6**	2022/09/24

A Calibrated Blackbody Source for Testing Next-Generation Wavefront Actuators

Phoebe Zyla

California Institute of Technology
LIGO Project, MS 18-34
Pasadena, CA 91125
Phone (626) 395-2129
Fax (626) 304-9834
E-mail: info@ligo.caltech.edu

Massachusetts Institute of Technology
LIGO Project, Room NW22-295
Cambridge, MA 02139
Phone (617) 253-4824
Fax (617) 253-7014
E-mail: info@ligo.mit.edu

LIGO Hanford Observatory
Route 10, Mile Marker 2
Richland, WA 99352
Phone (509) 372-8106
Fax (509) 372-8137
E-mail: info@ligo.caltech.edu

LIGO Livingston Observatory
19100 LIGO Lane
Livingston, LA 70754
Phone (225) 686-3100
Fax (225) 686-7189
E-mail: info@ligo.caltech.edu

http://www.ligo.caltech.edu/

1 Abstract

To lower the quantum noise floor and enhance sensitivity, aLIGO's power must be increased. However, defects within aLIGO's test masses due to the thermal effects of the laser prevent this. The current solution for this is to use a thermal compensation system (TCS) which includes a ring heater adaptive optics device. The aLIGO test masses react to the ring heater and are corrected to minimize scattering into higher order modes. The precision of the TCS can be improved with assurance that the thermal imaging system is accurate and that the real incident radiance profile of the test mass matches the theoretical expectations. This is tested with an in-air IR test facility consisting of a simple radiation source projecting onto a highly absorptive thin screen. With a simple heater geometry that emulates the ring pattern of the TCS adaptive optics, end-to-end of experimental data measured by an IR camera's code is provided. The incident radiance profile of the test masses as well as the power transfer from the heater to the screen may be analyzed, and the same calibration, once validated, may be used for more complex geometries in the future.

2 Introduction

LIGO (Laser Interferometer Gravitational-wave Observatory) was built to detect gravitational waves with two interferometers. The gravitational waves advanced LIGO (aLIGO) detects distort space as they move through space, which can be detected by measuring extremely small distances. For aLIGO, the size of interference measurements caused by gravitational waves is on the order of 10^{-18} meters. aLIGO currently can only observe gravitational events that are extremely large in magnitude, as the waves lose most of their magnitude while traveling through space. The type of events that can be observed are the collisions of two black holes, and the merging of two neutron stars. In improving aLIGO's sensitivity, we will be able to detect smaller amplitude signals; we will see more events within a given volume and more signals from farther out. The main issue facing this currently is that the arm power could be moved much closer to the design power [Figure 1]. A large part of this improvement is perfecting the surfaces of the test masses in the interferometer to minimize noise due to manufacturing errors. As shown in Figure 1, the blue dashed line representing the input laser power is linear, while the actual arm power levels off at a certain wattage. To fix this, the test masses must be further improved.

Currently, aLIGO has a thermal compensation system that aims to reduce loss due to thermal noise [6]. Part of this is a system of ring heaters which sit around the barrels of the test masses, and heat the TMs in order to reduce central distortion due to the heat of the laser. To do this, the ring heaters must overcompensate further out from the center of the TMs, which results in larger distortions around the edges of the TMs [Figure 2]. As seen in this figure, the center area of the test masses are flattened out, but the edges experience a large amount of deformation. The fundamental Gaussian mode of the laser only impacts a small central circle of the test masses, so as long this circle is not distorted on the TMs, the laser power will not be negatively affected. The more power that is used with these current ring heaters will result in more surface deformation of the TMs closer to the center, which becomes an issue when the area the ideal Gaussian mode hits is no longer being flattened.

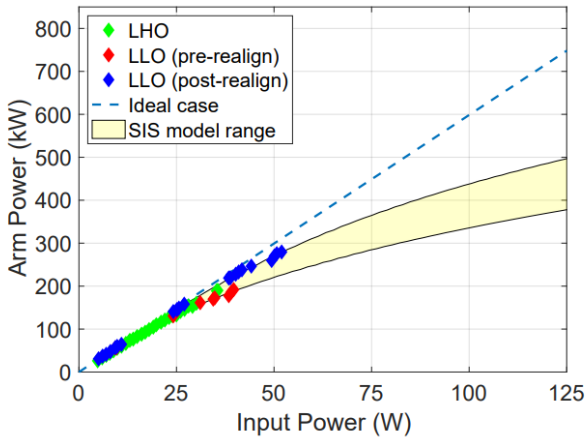

Figure 1: Arm power versus input laser power (Brooks *et al.*, P1900287)

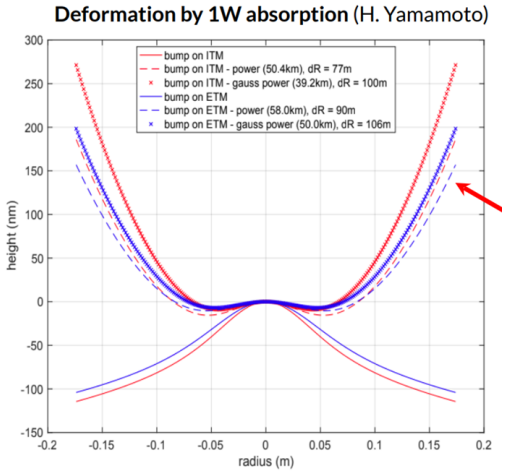

Figure 2: Residual deformation after ring heater correction

The limitations of this ring heater design become clear as aLIGO's laser power is increased. When the test masses are manufactured, point absorber defects will occasionally be trapped between the coating layers, making them impossible to remove [5]. The laser light will scatter when it hits these point defects and will enter higher order modes (HOMs), resulting in a large power loss. It becomes extremely difficult to continue to increase laser power as the laser scatters into HOMs, resulting in the flattening of the Arm power curved in Figure 1. Specifically for aLIGO, the 7th order mode of the laser has strong resonance within the arm cavities [Figure 3]. There is a strong degeneracy between the 7th OM and the 0-0 mode, and as the equation for power loss due to a specific mode depends on the single bounce scattering coefficient L_o and the gain of the mode, we must find a way to change the gain of the 7th OM.

$$Loss_{00,mn} = L_o * Gain_{mn}$$

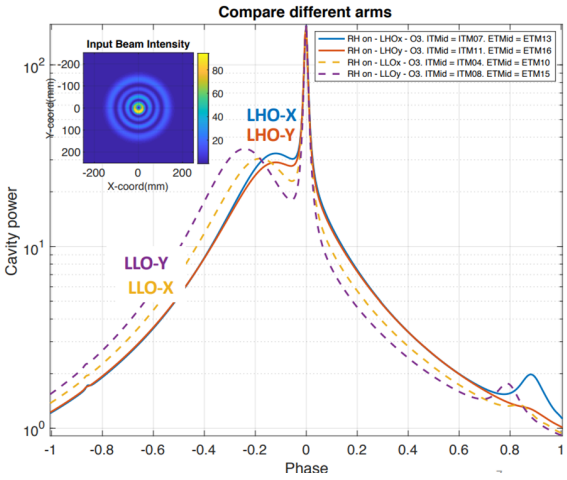

Figure 3: Resonance between the 7th OM and the 0-0 mode

The point absorbers themselves as well as the HOMs cannot be compensated for with the current simple ring heater. With Dr. Richardson's proposed next generation ring heater actuators, we will be able to address the 7th OM and greatly reduce the loss due to scattering. The 7th OM has a much large profile than the 0-0 mode, so the outer ring of the test masses may be deformed to shift the 7th OM without affecting the ideal Gaussian mode of the laser. The goal of the HOM ring heater is to not only reduce optical loss due to the 7th OM, but additionally to correct the affects of point absorbers with a segmented heating approach. This will be more effective than the current ring heaters, and will move the aLIGO arm power closer to the design power.

3 Objectives

The main objective of this project is to validate our system calibration by calculating the theoretical incident radiance profile of the test mass and experimentally fitting our calibration. We will design and measure a calibrated black body source, and fit the calibration with data and theoretical calculations. There will be end-to-end validation of the system calibration to allow for future prototypes and more complex black body sources.

4 Method

4.1 Optical Table Setup

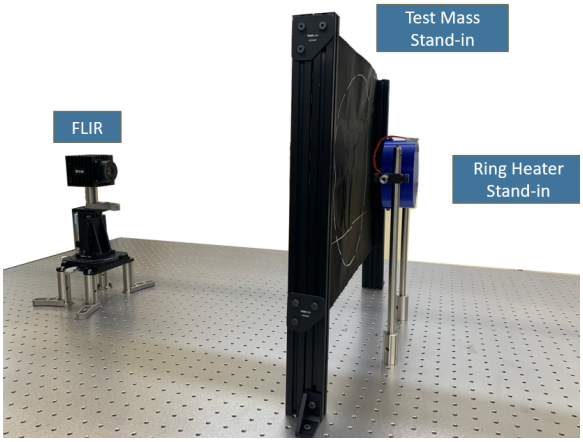

Figure 4: Optical Table Setup Diagram

To begin, the test mass was first mounted onto the table. Our test mass consists of four 20 cm by 60 cm highly reflective metal velvet foil sheets, put together to create a two-sided 40 cm by 60 cm sheet. This is held in place by 20' optical posts, so that the top of the sheet is equal to the top of the posts. Each side of the sheet will have two posts clamped together to hold up the sheet with pressure only.

The IR camera has a field of view of 51 degrees, and the test mass has a height of 40 cm, so the IR camera must be 41.9 cm, or 16.4 inches, away from the test mass. The mounting of

the camera is much simpler than the test mass, as it can directly screw into a stand which can be connected directly to the optical table.

The heater system for this project is a small cylindrical cartridge heater suspended in a parabolic reflector. The cartridge heater, which is 20 mm long and 6 mm in diameter, is held so that its heated end is at the reflector's focal point, and the main body of the heater blocks additional radiation off of the heater. Because we are working with a parabolic reflector, ideally the heater would be a point source at the focal point. This is not possible, so the solution to extra unwanted rays will be this orientation of the heater. The reflector, which has a height of 45 mm, a length of 100 mm, and a focal point of 12.5 mm, will be positioned very close to the test mass, to minimize the occlusion of rays. The rays hit the test mass in a predictable circular shape for our end-to-end validation of the power transfer.

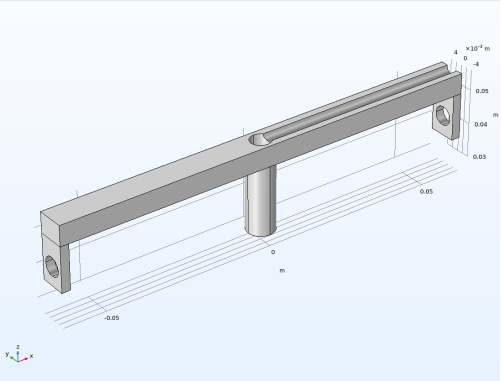

Figure 5: Heater Bridge Model

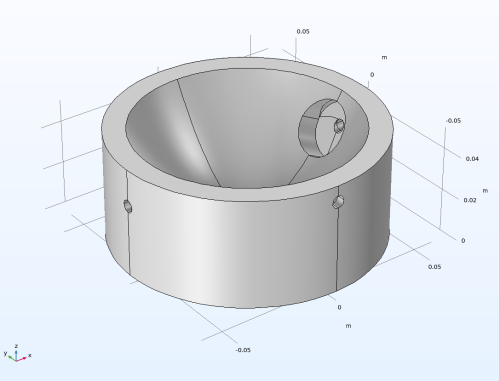

Figure 6: Reflector Mount Model

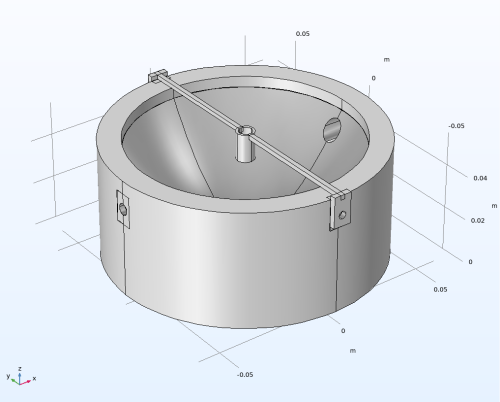

Figure 7: Full Mount Model

It was decided to use a parabolic reflector because it would create a circular shape similar to the ring heater of the TCS, but would not take as long to acquire. The physics of a parabolic reflector are well-understood and the theoretical calculations will not be hugely difficult as well. A cartridge heater was the best option for our use, as they are small and affordable, and for a parabolic reflector we want a heat source as close to a point source as possible. We are also using a thermocouple to measure the temperature of the heater. The thermocouple acts as another method of ensuring that our measurements are correct. If the measured irradiance of the test mass did not agree with the measured temperature of the heater, then we would know that there is a problem with the power transfer or with our

theoretical calculations.

To hold the cartridge heater exactly at the reflector's focal point, a mount was 3D printed for the entire system. This mount was designed using COMSOL, and there are two parts to this mount: a bowl-shaped holder for the reflector itself [Figure 6], as well as a bridge across this bowl for the heater to sit in [Figure 5]. Both parts are attached to an optical table with 1/2" optical components. The reflector mount fit the reflector precisely enough that only the bridge going across is needed to hold it in place. There is some difficulty here, as the manufacturers of the parabolic reflector did not provide a CAD model of the reflector nor measurements of the outer profile of the reflector; the only known measurements are of the inner reflective surface. Due to this uncertainty, multiple iterations of the printed mount were needed to ensure correct fit of the reflector. The mount, once printed, was held in place by two counterbores on the right and left of the reflector, which screws into an optical component clamp. The component clamp was held in place by two optical posts, connected with a right-angle post clamp. These were all set so that the center of the reflector is held at 308 mm above the table, where the center of the test mass was. The bridge for the heater was positioned vertically across the reflector mount, and was screwed directly into the reflector mount. The bridge was as thin as possible, so as to obstruct as few rays as possible from the reflector, while still thick enough to be printed. The printer we used could print objects with a minimum width of 1 mm. There is a small hole in the center of the heater bridge that will hold the wires of the cartridge heater as well as the thermocouple wires, and acts as a clamp onto the heater.

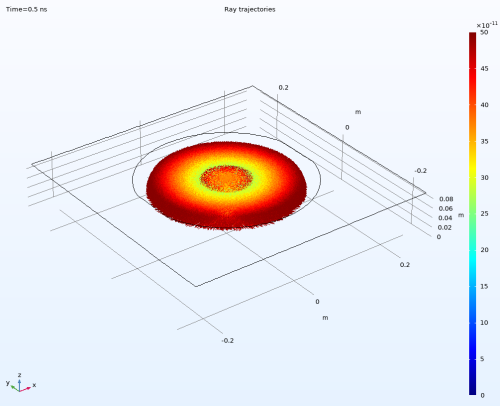

Figure 8: COMSOL Ray Diagram

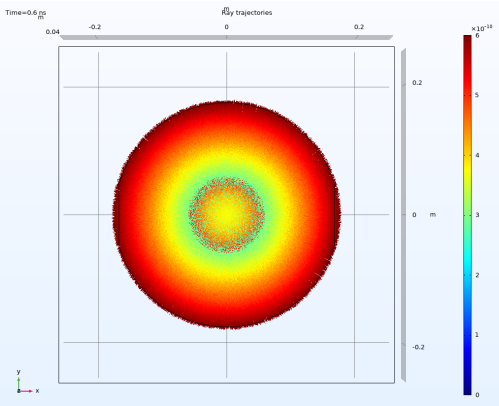

Figure 9: Ray Diagram 2

4.2 COMSOL Modeling and Theoretical Calculations

Once the table is fully set up, we began calculating the theoretical power transfer from the heater system to the test mass. This was done with consideration to the ray diagrams of the cartridge heater in the parabolic reflector, the inverse square law of power transfer, and Wien's displacement law. While some calculation were done by hand (namely the projected power output of the cartridge heater and the estimated irradiance pattern projected onto the test mass), the majority of these calculations with be done with COMSOL's geometrical optics modeling. The model consists of the heater, the reflector, and a target plane functioning as the test mass. The heater radiates from all surfaces except the surface facing

directly towards the test mass, as this surface is wired and not made of the same metal as the rest of the heater. One difficulty here was determining the exact material of the heater; the manufacturer lists it only as stainless steel and does not provide the properties. After many tests, it was determined that the emissivity of the heater was 0.57, which is in-line with known emissivity values for machine-polished 304 stainless steel [22]. As an additional point of validation, the power dissipated by the heater was equated to the power radiated by the heater. The conducted power was determined to be negligible, as it was conducted only to the atmosphere.

$$P_{dissipated} = P_{radiated} + P_{conducted}$$

The dissipated power, being equal to the input power divided by the resistance of the heater, would be easily determined. The radiated power would be equal to a form of Stefan-Boltzmann's law, allowing for the emissivity of the heater to be determined. For this, A is the area of the heater actively radiating, T is the temperature the heater is measured at, T_o is the ambient temperature of the atmosphere, and ϵ will be the emissivity of the heater.

$$fracI * VR = A * \sigma_{SB} * (T^4 - T_o^4) * \epsilon$$

This emissivity was then input into COMSOL so as to accurately model how the heater irradiated onto the target plane.

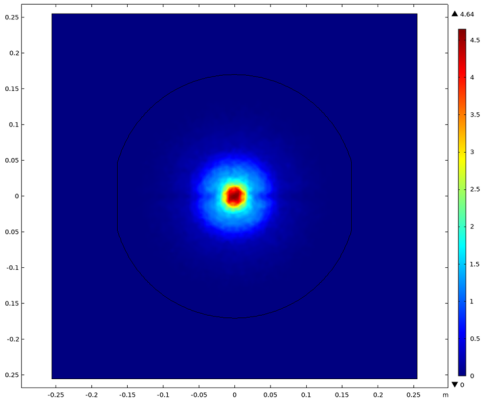

Figure 10: Irradiance Map

The inner surfaces of the reflector act as a mirror, and have a coating of polished aluminum. The outer surfaces of the mirror do not interact with the rays directly, and act as a wall. The bulk of the reflector is made of BOROFLOAT, a substance used by Edmund Optics. The target plane also acts as a wall, and is where the deposited ray power is calculated. From this calculation we could determine the accuracy of the experimental results. The COMSOL modeling provided us with a ray diagram [Figures 8, 9] as well as an irradiance map of the test mass [Figure 10]. There is some spreading of the rays in the irradiance maps, as expected as the heater is not a perfect point source. The maximum irradiance on the screen from the heater based on these models should be 4.65 W/m^2, and using a modified form of the Stefan-Boltzmann law with an absorptivity of 0.99, the theoretical maximum temperature of the can be found. For this, the maximum irradiance on the screen was used for E_e.

$$T = (\frac{E_e}{\epsilon * \sigma_{SB}} + T_o^4)^{1/4}$$

This calculation gave the value of 28 ± 1^oC as the maximum temperature the screen should reach when being irradiated onto.

4.3 Real Data

The first week of taking real data began with ensuring that the thermocouple was calibrated correctly and connected securely to the cartridge heater, which was done using Kapton tape. The testing consisted of comparing the thermocouple's measured temperature with the FLIR's measured temperature. Initially it was thought that the heater had a hot spot in its middle, but this was simply the Kapton tape, which has a very different emissivity than the stainless steel of the heater. The voltage, current, thermocouple temperature, FLIR temperature, and the time the heater took to stabilize were noted down. After it was certain that any measured temperature fluctuations were due to intermittent contact with the thermocouple and that the heater's resistivity did not change over time, the heater was moved in front of the target screen to begin testing.

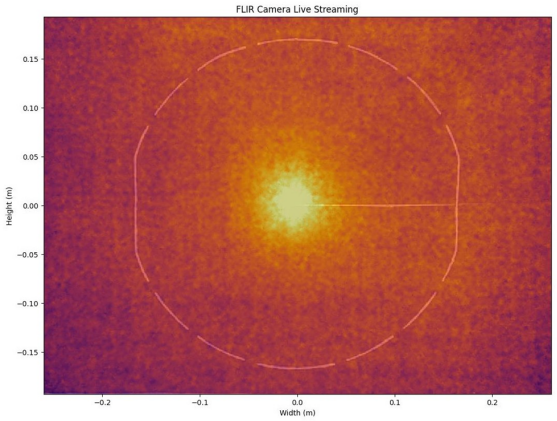

Figure 11: Measured Irradiance from the FLIR

In order to prevent overheating of the screen, the input current was increased in increments of $0.01A$, allowing the heater to come to thermal equilibrium in between each increase. Over multiple trials, it was found that when $1W$ of power was run through the heater, the heater would reach a temperature of about 110^oC, and the target screen would reach a maximum temperature of 29 ± 1^oC. This matches the expected temperature of the other side of the screen, proving that there is little thermal loss between the two sides of the screen. The shape of the FLIR's measured irradiance map also closely matches the COMSOL model [Figure 11]. In knowing that the values for COMSOL model and the real-world measured irradiance map are similar enough, the optical table setup is validated, as well as the calibration for the FLIR.

5 Summary and Next Steps

The system has been validated and the in-air optical test facility is ready to be used to test the prototype HOM ring heater being developed by the Richardson lab. The system has a functioning IR camera coded and setup by Cassidy Nicks and Tyler Rosauer [14]. In the future, this new ring heater will address the flaws and limitations in the current ring heater design, which will allow for an increase in aLIGO's laser power and overall instrument sensitivity.

6 Acknowledgements

I would like to acknowledge the NSF, UC Riverside, the Caltech SURF program, and LIGO laboratory. I would also like to thank my mentor, Ryan Andersen, as well as my PI, Dr. Jon Richardson for their guidance and support

References

[1] Abbott, B P, *et al.* "LIGO: The Laser Interferometer Gravitational-Wave Observatory." *Reports on Progress in Physics*, vol. 72, no. 7, 2009, p. 076901., https://doi.org/10.1088/0034-4885/72/7/076901.

[2] "Award Abstract 0969935 Research on the Thermal Correction System and Thermal Coating Noise." NSF AWARD, 30 Sept. 2010, https://www.nsf.gov/awardsearch/showAward?AWD_ID=0969935&HistoricalAwards=false.

[3] Ballmer, Stefan W., and For the Collaboration. "Noise Couplings in the Laser Interferometer Gravitational Wave Observatory (LIGO)." *Frontiers in Optics 2007/Laser Science XXIII/Organic Materials and Devices for Displays and Energy Conversion*, 2007, https://doi.org/10.1364/ls.2007.lma2.

[4] Barish, Barry C., and Rainer Weiss. "LIGO and the Detection of Gravitational Waves." *Physics Today*, vol. 52, no. 10, 1999, pp. 44–50., https://doi.org/10.1063/1.882861.

[5] Brooks, Aiden, *Point Absorbers Observations and Effects*. LIGO-G2200064-v2, (2022).

[6] Brooks, Aiden, *et al.* "Overview of Advanced LIGO Adaptive Optics." *Applied Optics,* vol. 55, no. 29, 2016, pp. 8256-8265., https://doi.org/10.1364/AO/55.008256.

[7] Brooks, Aiden, *et al. Point Absorbers in Advanced LIGO*. LIGO-P1900287.

[8] Brooks, A., Vajente, G., Yamamoto, H., *Higher order mode ring heater to suppress point absorber loss: Initial Concept*. LIGO-G2000874-v3, (2020).

[9] Chu, Jennifer. "GW170817 Press Release." *Caltech*, https://www.ligo.caltech.edu/page/press-release-gw170817.

[10] Day, Richard. "Central Radius of Curvature Correction System (CHRoCC) Used in Virgo." *Virgo/GEO Commissioning Meeting*, Sept 2011.

[11] Day, R. A., *et al.* "Reduction of Higher Order Mode Generation in Large Scale Gravitational Wave Interferometers by Central Heating Residual Aberration Correction." *Physical Review D*, vol. 87, no. 8, 2013, https://doi.org/10.1103/physrevd.87.082003.

[12] Harry, G., *Advanced LIGO Test Masses and Core Optics*. LIGO-G1000098-v2, (2010).

[13] "LIGO - a Gravitational-Wave Interferometer." Caltech, LIGO Caltech, https://www.ligo.caltech.edu/page/ligo-gw-interferometer.

[14] Nicks, C., Rosauer, T., Richardson, J., *Developing an In-Air IR Test Facility for Next-Generation Wavefront Control*. LIGO-T2200205, (2022).

[15] Reitze, David, *The Future of Ground-based Gravitational-wave Detectors*. LIGO-G1800292-v1, (2018).

[16] Richardson, Jon, *Active Wavefront Control for Megawatt Arm Power*. LIGO-G2200399, (2022).

[17] Richardson, Jon. "Experimental Gravitational Physics at UC Riverside", 15 July 2021.

[18] Richardson, Jon, *et al.* "Developmental Status of the Higher-Order Mode Ring Heater", 2 March 2022.

[19] Richardson, J., Brooks, A., *Higher Order Mode Ring Heater Overview*. LIGO-G2101232-v4, (2021).

[20] "Stainless Steel - Grade 304." *Consultancy*, https://www.dm-consultancy.com/TR/dosya/1-59/h/aisi-340-info.pdf.

[21] Steinlechner, J. "Development of Mirror Coatings for Gravitational-Wave Detectors." *Philosophical Transactions. Series A, Mathematical, Physical, and Engineering Sciences*, The Royal Society Publishing, 28 May 2018, https://www.ncbi.nlm.nih.gov/pmc/articles/PMC5915647/.

[22] "Table of Emissivity of Various Surfaces." *Transmetra*, https://www.transmetra.ch/images/transmetra_pdf/publikationen_literatur/pyrometrie-thermografie/emissivity_table.pdf.

[23] Willems, P., Brooks, A. *Advanced LIGO Thermal Compensation System Preliminary Design*. (2008).

[24] Yamamoto, Hiro, *Cause and effect of point absorbers on test masses – modeling*. LIGO-G2000282-v3, (2020).